Bendola Publishing
Journal of Transition Metal Complexes
Vol. 5 (2022), Article ID 246138, 14 pages
doi:10.32371/jtmc/246138

Research Article

Synthesis, Characterization, Biological Activity and Solid-State Electrical Conductivity Study of Some Metal Complexes Involving Pyrazine-2-Carbohydrazone of 2-Hydroxyacetophenone

Ashish Bansod, Ravindra Bhaskar, Chandarshekhar Ladole, Nilesh Salunkhe, Kanchan Thakare, and Anand Aswar

Department of Chemistry, Sant Gadge Baba Amravati University, Amravati, Maharashtra 444602, India
Address correspondence to Anand Aswar, aswaranand@gmail.com

Received 13 November 2021; Revised 20 March 2022; Accepted 28 March 2022

Abstract A novel hydrazone Schiff base ligand N'-(1-(2-hydroxyphenyl)ethylidene)pyrazine-2-carbohydrazide (H_2L) and its Ti(III), Cr(III), Fe(III), WO_2(VI), Th(IV), and UO_2(VI) metal complexes were synthesized. The complexes were characterized by elemental analyses, magnetic susceptibility measurements, IR, reflectance spectra, thermal analysis, powder X-ray diffraction, and SEM analysis. The elemental analyses suggest 1:1 metal–ligand stoichiometry for all the complexes. The ligand coordinates as dibasic tridentate manner towards central metal ions through ONO donor sequence forming a five- and six-member chelating ring. Based on the physico-chemical studies, monomeric octahedral geometry has been suggested for all the complexes. Various kinetic and thermodynamic parameters have been evaluated from the thermal data by using Coats-Redfern equation. The solid-state electrical conductivity was measured in their pellet form over a temperature range 313–373 K and all the compounds showed semiconducting behavior as their conductivity increases with increase in temperature. The ligand and its complexes were screened in vitro for their biological activity against *E. coli* MTCC 443; *P. aeruginosa* MTCC 424; *S. aureus* MTCC 96; *B. subtilis* MTCC 8979; *E. faecalis* MTCC 439; *S. pyogenes* MTCC 442; fungal strains *C. albicans* MTCC 227, *A. niger* MTCC 282, and *A. clavatus* MTCC 1323; and all the complexes showed better biological efficacy than the free ligand.

Keywords pyrazine-2-carbohydrazone; metal complexes; TGA; electrical conductivity; biological activity

1. Introduction

Hydrazones are characterized by the presence of the triatomic grouping $-C=N-N-$ and are found as interesting ligands in coordination chemistry due to their strong chelating ability through the electron delocalization, which is attached with extended conjugation, structure diversity and a wide range of possible applications [1, 2, 3]. Hydrazones and hydrazides have also gained considerable interest in recent years owing to their wide variety of biological and pharmacological properties as well [4, 5]. Hydrazone Schiff bases continue to attract attention of several investigators due to their diverse biological applications like antimicrobial [6], antifungal [7], anticancer [8], herbicidal [9], and so forth. The metal complexes of hydrazones including heterocyclic moieties involving nitrogen, oxygen and sulphur as coordinating functionalities have been studied extensively in order to establish a relationship between the chemical structure and biological activity [10, 11, 12, 13]. Earlier, we reported few metal complexes of biologically active hydrazone Schiff bases and compounds that showed interesting electrical and biological properties which prompted us to extend further our work with higher-valent metal ion complexes of pyrazine carbohydrazone of 2-hydroxyacetophenone to see metalation effect on such properties compared to substituted analog [14, 15]. Considering the importance associated with pyrazine-2-carbohydrazide, in the present study we describe synthesis and characterization of Ti(III), Cr(III), Fe(III), WO_2(VI), Th(IV) and UO_2(VI) complexes with the ligand N'-(1-(2-hydroxyphenyl)ethylidene)pyrazine-2-carbohydrazide (H_2L) derived from the condensation reaction of 1-(2-hydroxyphenyl)ethan-1-one with pyrazine-2-carbohydrazide (Scheme 1). After physicochemical characterization, these compounds were evaluated for their antibacterial and antifungal activities. Further, solid-state electrical conductivity of compounds has also been measured.

2. Experimental

2.1. Materials

The chemicals used were all analytical reagent grade or chemically pure grade. Pyrazine-2 carboxylic acid and 1-(2-hydroxyphenyl)ethan-1-one (99%) (Aldrich Chemical Company, USA), acetylacetone, hydrazine hydrate (98%), anhydrous titanium chloride (99%), chromium chloride hexahydrate (96%), anhydrous ferric chloride (97%), thorium nitrate pentahydrate (99%), and uranyl nitrate hexahydrate (99%) were of analytical reagent grade, obtained from SD Fine Chemicals, Mumbai, India and

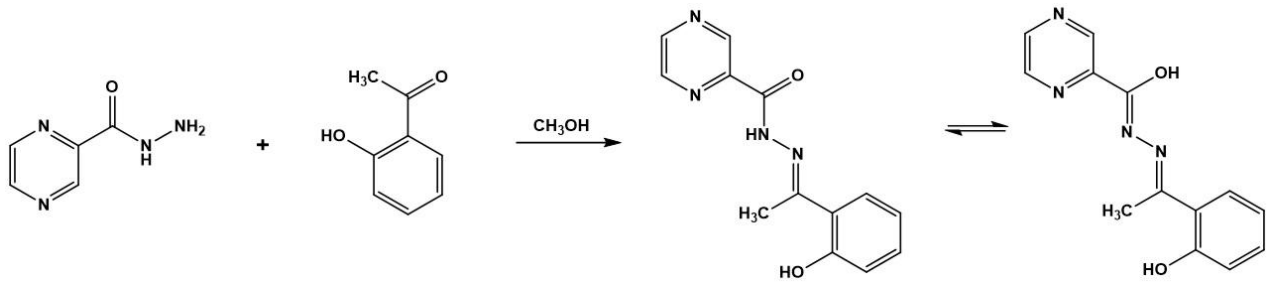

Scheme 1: Synthesis and tautomeric forms of H_2L ligand.

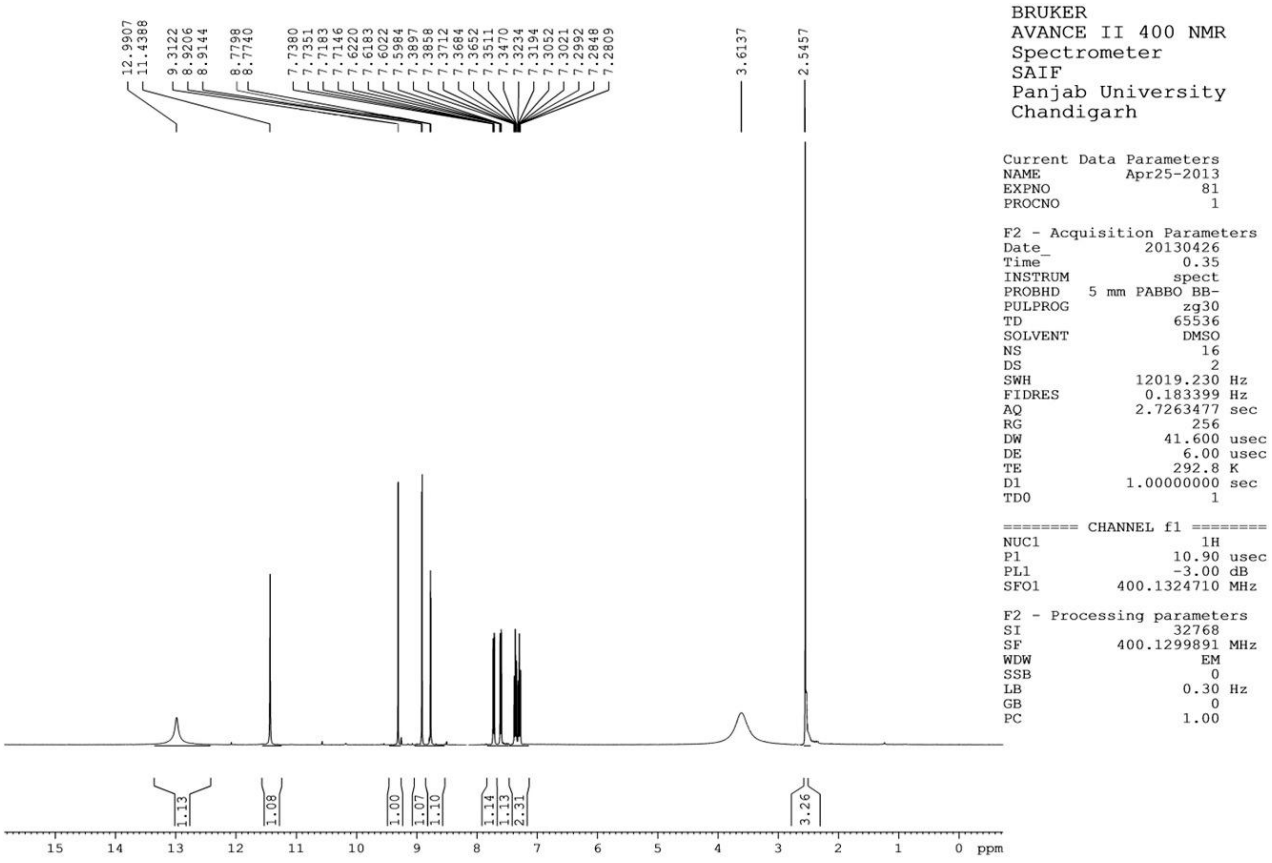

Figure 1: ^{1}HNMR spectrum of H_2L ligand.

were used as supplied (99% purity). Solvents employed were either of 99% purity or purified by known literature methods [16,17]. $WO_2(acac)_2$ was prepared according to literature methods [18].

2.2. Physical measurements

Micro analyses of carbon, hydrogen, and nitrogen of the complexes were obtained using a Carlo Erba 1108 elemental analyzer. The IR spectra were recorded as KBr pellets using a Shimadzu 8201 spectrophotometer in the range 400–4000 cm^{-1}. The metal and chloride contents were determined gravimetrically [15]. ^{1}H and ^{13}C NMR spectra of ligand were recorded on Bruker Advance II 400 MHz NMR spectrometer in DMSO-d_6 using TMS as an internal standard. Magnetic measurements were carried out by the Sherwood magnetic susceptibility balance MK-1 at room temperature. The solid-state reflectance spectra of the complexes were recorded in the 200–1200 nm range using MgO as diluent on a Cary 60 UV-Vis spectrophotometer. Thermogravimetric analyses were performed on a Perkin Elmer, Diamond TG thermal analyzer in the temperature range 40–750 °C at a heating rate of 10 °C min^{-1} under a dynamic air atmosphere. X-ray diffraction patterns were obtained with a Bruker AXS, D8 Advance X-Ray

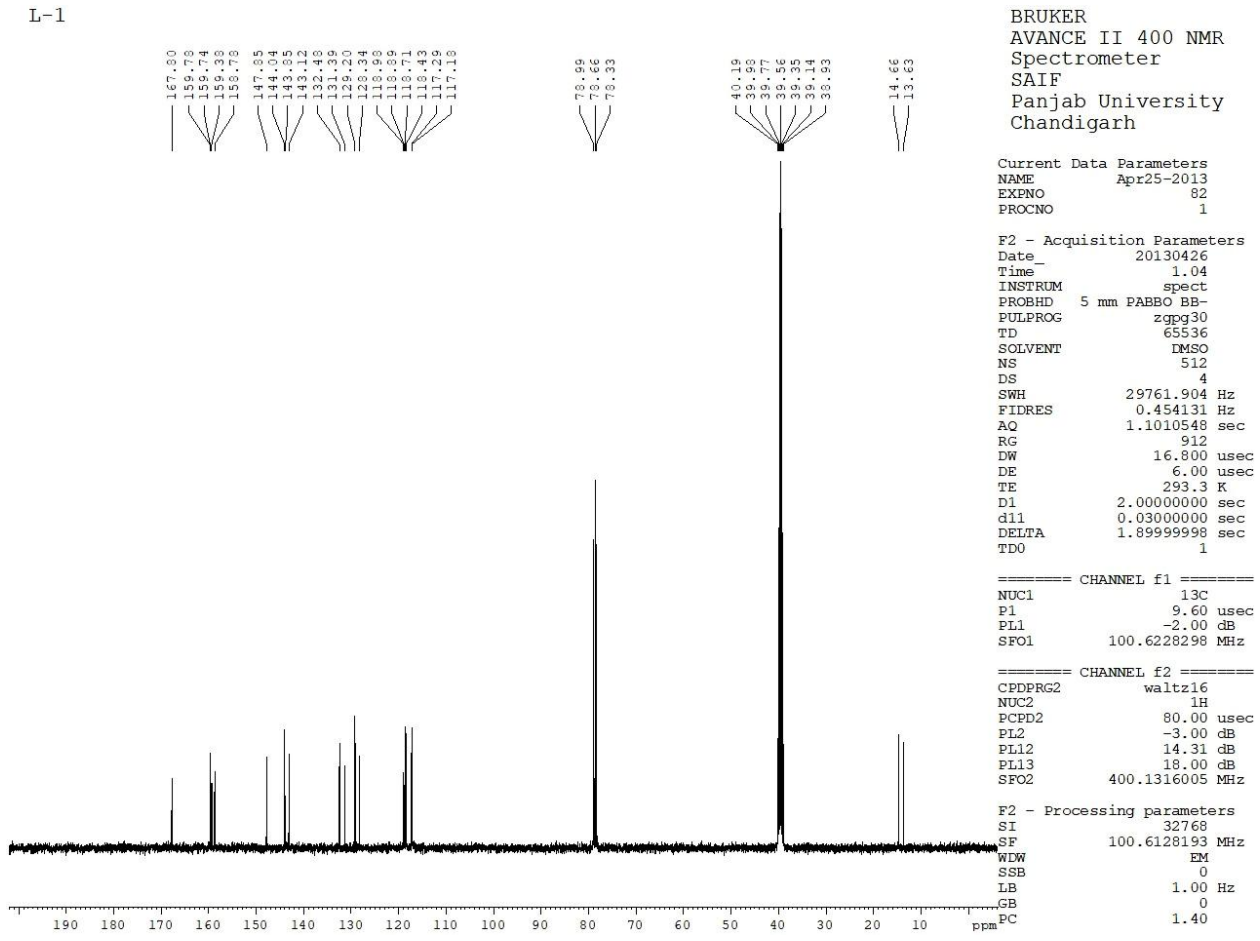

Figure 2: ^{13}C NMR spectrum of H_2L ligand.

diffractometer equipped with Si(Li) PDS. Mass spectrum of ligand was recorded on a Waters, Q-TOF micro mass (LC-MS) spectrometer. The surface morphology was observed using a JEOL Model JSM-6390LV scanning electron microscope. The solid-state electrical conductivity was measured as a function of temperature (313–373 K) in their compressed pellet form by using two probe methods. All the samples were compressed to pellets (13 mm dia × 1 mm) using a pressure of 3 ton cm^{-2}. In order to provide a better electrical contact between pellet and electrodes, both surfaces of pellet were polished by silver paste and placed between two copper electrodes. The temperature of the sample was measured with the accuracy ±1 °C with a calibrated nichrome thermocouple inserted inside the cell. The activation energies of electrical conductance were calculated using Arrhenius equation $\sigma = \sigma^0 \exp(\mathrm{Ea/KT})$.

2.3. Synthesis

2.3.1. Synthesis of the ligand H_2L

The ligand N'-(1-(2-hydroxyphenyl)ethylidene)pyrazine-2-carbohydrazide (H_2L) was prepared according to the previously reported method [19]. The chemical structure of ligand was confirmed by various spectral characterizations (IR, ^{1}H, ^{13}C NMR, and mass spectra). The ligand has been synthesized under double stage synthesis and its synthetic scheme has been shown in Scheme 1.

Micro-analytical data for $C_{13}H_{12}N_4O_2$. Anal. Calc., C, 60.93; H, 4.72; N, 21.86. Found C, 61.12; H, 4.70; N, 21.83%. IR (KBr disc, cm^1), 3,346 (OH), 3,182 (NH), 1,691 m(C=O), 1,630 m(C=N), 1,301 (C−O).

2.3.2. Synthesis of complexes

All the metal complexes [except WO_2(VI)] were prepared in a similar way by the following general method. Equimolar quantities of metal salts (1 mmol) and ligand (H_2L) (2.57 g, 1 mmol) were dissolved separately in DCM + MeOH (50:50 v/v) (∼ 25 mL) and both solutions were filtered and mixed in warm condition. The reaction mixture was refluxed for 5–6 h on a water bath. The pH of the reaction mixture was adjusted ∼ 6–7 by adding methanolic solution of sodium acetate (∼ 0.5 g) and refluxed further for another 1 h and then cooled to the room temperature. The solid product in each case was filtered off; washed several times

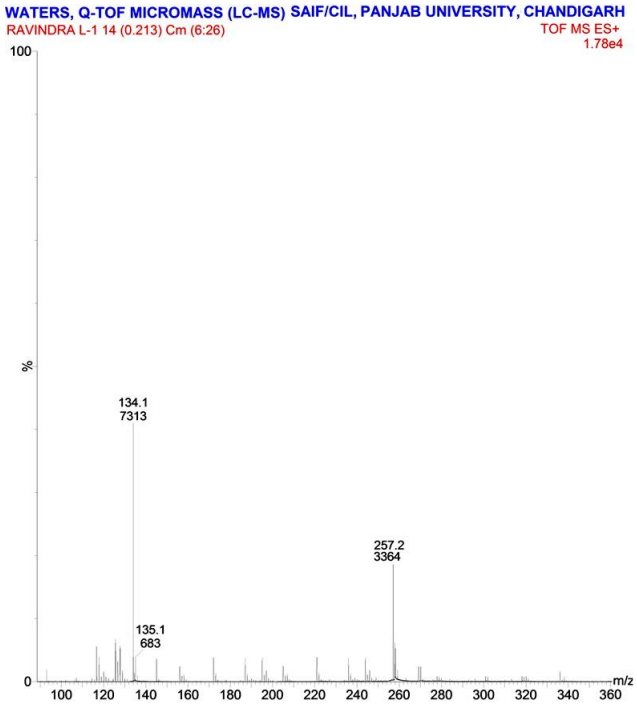

Figure 3: Mass spectrum of H_2L ligand.

with cold DCM, methanol, and petroleum ether; and dried under vacuum over $CaCl_2$. Yield, 65–68%.

2.3.3. Synthesis of [$WO_2(L)H_2O$] complex

A hot solution of [$WO_2(acac)_2$] (0.34 g, 1 mmol) in ~ 25 mL of methanol was added dropwise to a methanol (25 mL) solution of N'-(1-(2-hydroxyphenyl)ethylidene)pyrazine-2-carbohydrazide (H_2L) (2.57 g,1 mmol) with continuous vigorous shaking. The resulting turbid solution obtained was filtered and then further refluxed on a water bath for 6 h. After reducing volume of the solution to *Ca* 10 mL and cooling to 10 °C overnight, the separated colored solid was filtered, washed with methanol followed by petroleum ether, and finally dried in desiccator over silica gel. Yield, 67%.

2.4. Antimicrobial activity

The Schiff base ligand (H_2L) and its complexes were screened for their anti-bacterial and anti-fungal activity against *E. coli* MTCC 443, *P. aeruginosa* MTCC 424, *S. aureus* MTCC 96, *B. subtilis* MTCC 8979, *E. faecalis* MTCC 439, *S. pyogenes* MTCC 442, and fungal strains such as *C. albicans* MTCC 227, *A. niger* MTCC 282, and *A. clavatus* MTCC 1323 by using disc-agar diffusion method [20]. The solutions of ciprofloxacin (antibacterial drug) and clotrimazole (antifungal drug) were used as standard. Minimum inhibitory concentrations (MICs) of the compounds against test organisms were determined by the broth microdilution method [21,22,23,24] and DMSO was used as a negative control. All these tests were performed

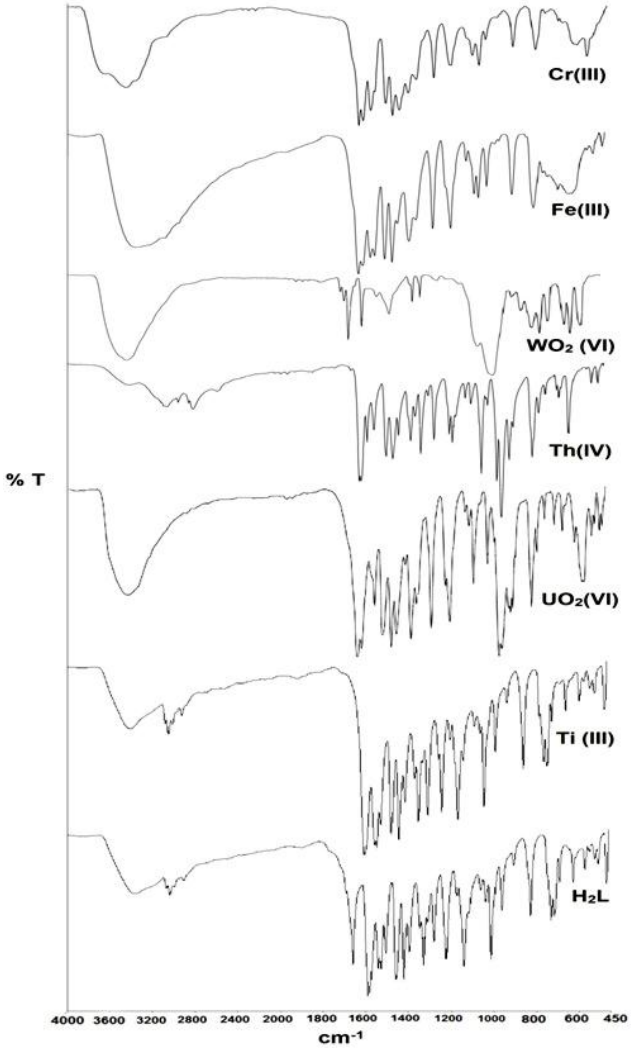

Figure 4: IR spectra of H_2L ligand and its complexes.

three times under identical conditions and average values were recorded. Activity was determined by measuring the diameter of zone showing complete inhibition and has been expressed in mm.

3. Results and discussion

The reaction between pyrazine-2-carbohydrazide and 1-(2-hydroxyphenyl) ethan-1-one in ethanol yields a new hydrazone Schiff base ligand (H_2L) [19]. The formation of ligand was confirmed by elemental and spectral data. The ^{1}HNMR spectrum of ligand exhibits two resonances at 11.43 ppm and 12.99 ppm (singlet, 1 H each) due to NH and phenolic protons, respectively. A sharp signal observed at 2.54 ppm due to the methyl protons of the hydroxyl acetophenone moiety indicates the formation of ligands. The mass spectrum of ligand showed a molecular ion peak at $m/z = 257$ which is consistent with its formula weight. Reaction of this ligand with metal salts resulted

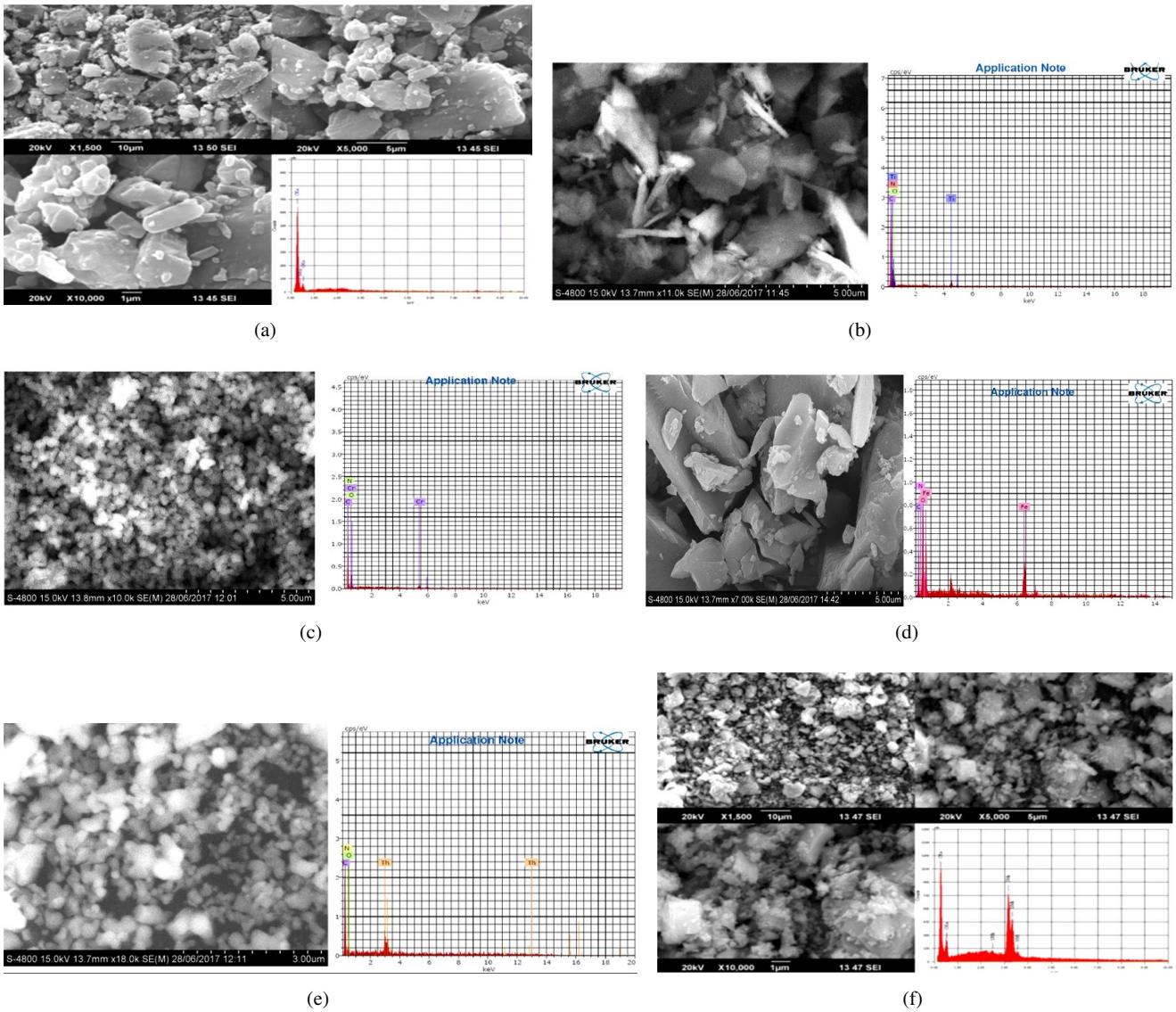

Figure 5: Scanning electron microscope images of (a) H_2L ligand, (b) $[Ti(L)(Cl)(H_2O)_2]$ complex, (c) $[Cr(L)(Cl)(H_2O)_2]$ complex, (d) $[Fe(Cl)(H_2O)_2HL_2]$ complex, (e) $[Th(L)(H_2O)(NO_3)_2]$ complex, and (f) $[UO_2(L_1)(CH_3OH)]$ complex.

in the formation of complexes with good yield. All complexes are colored, stable at room temperature, and insoluble in common solvents such as ethanol, methanol, chloroform, benzene, cyclohexane, acetone and diethyl ether, but sparingly soluble in DMF and DMSO only. The elemental analyses suggest 1:1 metal–ligand stoichiometry for all the complexes and it is in good agreement with the proposed structures and geometry of complexes (Table 1). The insufficient solubility of the complexes, even in DMSO-d_6, has prevented us from carrying out ^{1}H NMR and UV-Visible solution studies of complexes.

3.1. IR spectra

The IR spectra of complexes are compared with that of the free ligand (H_2L) to find out the points of attachment of the ligand to the metal ions in their complexes and assigning the coordination mode. When compared to free ligand, its characteristic IR stretching frequencies of imine and carbonyl groups are shifted on complex formation. The characteristic ligand bands at 1,691 cm^{-1}, 3,182 cm^{-1} and 3,346 cm^{-1} due to C=O, NH and OH stretches respectively are not observed in the corresponding complexes, indicating the transformation of C=O and NH groups to the enolic form and their subsequent coordination to the metal ions through the deprotonation of phenolic and enolic hydrogen [25,26,27]. This has been further confirmed by the appearance of a new enolic band in the region 1,238–1,242 cm^{-1} due to ν(C−O) in the spectra of complexes. The enolization is favored by the stabilization of the anion by the conjugation with the $>$ C=N−N=C $<$ group. The

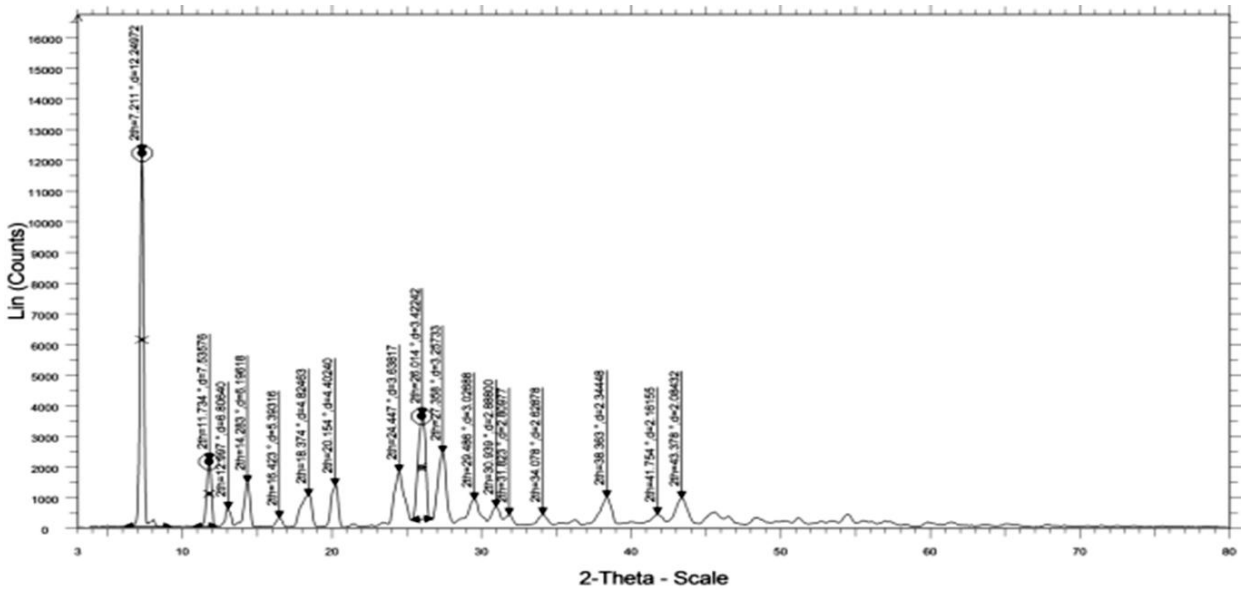

Figure 6: XRD diffractogram of ligand (H_2L).

Table 1: Physicochemical and dc electrical conductivity data of ligand and its metal complexes.

Compound	Color	Empirical formula & formula weight	Elemental analysis found (Calcd.) C	H	N	Cl	M	Solid-state electrical conductance σ (Ω^{-1} cm^{-1}) (at 40 & 100 °C)	Ea (eV)
H_2L	Reddish lemon	$C_{13}H_{12}N_4O_2$ 256.25	61.12 (60.93)	4.70 (4.72)	21.86 (21.83)	—	—	4.37×10^{-12} 3.90×10^{-11}	0.440
$[Ti(L)(Cl)(H_2O)_2]$	Dark umber	$C_{13}H_{13}ClN_4O_4Ti$ 373.59	41.75 (41.79)	3.75 (3.78)	14.95 (15.00)	12.75 (12.81)	9.45 (9.49)	1.62×10^{-12} 9.54×10^{-11}	0.766
$[Cr(L)(Cl)(H_2O)_2]$	Deep scarlet	$C_{13}H_{14}ClN_4O_4Cr$ 377.72	40.92 (41.34)	3.15 (3.74)	14.06 (14.86)	13.82 (13.77)	9.35 (9.39)	1.62×10^{-11} 9.54×10^{-10}	0.765
$[Fe(L)(Cl)(H_2O)_2]$	Umber	$C_{13}H_{14}ClN_4O_4Fe$ 381.57	40.37 (40.92)	3.68 (3.70)	14.53 (14.68)	14.60 (14.64)	9.25 (9.29)	7.34×10^{-10} 2.16×10^{-9}	0.748
$[WO_2(L)(H_2O)]$	Avocado	$C_{13}H_{12}N_4O_5W$ 488.10	33.06 (32.39)	2.01 (2.86)	11.90 (11.52)	—	37.08 (37.69)	7.32×10^{-11} 5.89×10^{-9}	0.856
$[Th(L)(NO_3)_2(H_2O)]$	Mustard	$C_{13}H_{12}N_6O_9Th$ 628.14	23.24 (24.84)	1.90 (1.91)	12.97 (13.37)	—	35.64 (36.94)	7.32×10^{-12} 5.89×10^{-10}	0.759
$[UO_2(L)(CH_3OH)]$	Terra cotta	$C_{13}H_{13}N_4O_4U$ 556.92	30.53 (30.73)	2.94 (2.61)	10.05 (10.27)	—	42.03 (42.87)	5.38×10^{-12} 3.65×10^{-10}	0.538

ligand exhibits a strong band at around 1,630 cm^{-1} due to ν(C=N) (azomethine), and this band has been shifted to lower frequencies in complexes by 31–33 cm^{-1}, indicating donation of the lone pair of electrons on azomethine nitrogen to metal center [28]. This has been strengthened by the upward shift of ν(N–N) band from 977 cm^{-1} to 1,021–1,038 cm^{-1} it the spectra of complexes also supported the coordination of the azomethine nitrogen atom to metal ions [29]. The $[UO_2(L)(CH_3OH)]$ complex exhibits bands at 900 (ν_3) cm^{-1} and 867 (ν_1) cm^{-1} assignable to ν_{asy}(O=U=O) and ν_{sym}(O=U=O) modes, respectively. The ν_3 value has been used to calculate the force constant (F) of ν(U=O) by the standard McGlynn et al. method [30]. The U−O bond distance is also calculated by the method of Jones [31]. The calculated F_{U-O} and R_{U-O} values are found to be 6.69 mdynes Å^{-1} and 1.74 Å respectively, showed in the normal range for most of uranyl complexes. The ν(C−O) band of CH_3OH is observed at 1,027 cm^{-1} and it showed a negative shift in UO_2(VI) complex and is observed at 992 cm^{-1}, indicating methanol is in coordination. The presence of a *cis*–WO_2 moiety in the complex WO_2(VI) may be inferred from the appearance of two bands in the 900–920 cm^{-1} region [32]. IR spectrum of Th(IV) complex shows two new non-ligand medium intensity bands at 1,425 cm^{-1} and 1,330 cm^{-1}, due to coordinated nitrate ion. All complexes (except UO_2(VI)) show broad bands at 3,338–3,432 cm^{-1}, 1,541–1,579 cm^{-1} and 836–863 cm^{-1} due to ν(OH), $\delta\gamma(H_2O)$, and $\delta w(H_2O)$ vibrations for the coordinated water molecules [33]. Further, the appearance of new bands in the 527–568 cm^{-1} and 462–492 cm^{-1}

Table 2: Infrared spectral bands (cm^{-1}) of the ligand and its metal complexes.

Compound phenolic (cm^{-1})	ν(OH...N)	ν(NH)	ν(C=O)	ν(C=N)	ν(C−O) phenolic	ν(C−O) enolic	ν(N−N)	ν(M−O)	ν(M−N)
H_2L	3,346	3,182	1,691	1,630	1,301	—	977	—	—
$[Ti(L)(Cl)(H_2O)_2]$	—	3,185	1,676	1,612	1,320	1,244	982	554	421
$[Cr(L)(Cl)(H_2O)_2]$	—	3,186	1,649	1,618	1,330	1,270	995	506	426
$[Fe(L)(Cl)(H_2O)_2]$	—	3,187	1,683	1,614	1,306	1,265	996	510	429
$[WO_2(L)(H_2O)]$	—	3,184	1,672	1,615	1,318	1,248	982	512	418
$[Th(L)(NO_3)_2(H_2O)]$	—	3,185	1,675	1,610	1,314	1,246	994	522	412
$[UO_2(L)(CH_3OH)]$	—	3,183	1,678	1,604	1,324	1,258	998	548	428

Table 3: Magnetic moments, electronic spectral data, and ligand field parameters of metal complexes.

Complex	μ_{eff} (B.M.)	Band position (nm)	Assignments	Dq (cm^{-1})	B_0 (cm^{-1})	β	ν_2/ν_1
$[Ti(L)(Cl)(H_2O)_2]$	1.87	532	$^2T_{2g} \rightarrow {}^2E_g$	—	—	—	—
$[Cr(L)(Cl)(H_2O)_2]$	3.97	580	$^4A_{2g} \rightarrow {}^4T_{2g}(F)$	1,724	709	0.77	1.44
		411	$^4A_{2g} \rightarrow {}^4T_{1g}(F)$				
		262	$^4A_{2g} \rightarrow {}^4T_{2g}(P)$				
$[Fe(L)(Cl)(H_2O)_2]$	5.91	833	$^6A_{1g} \rightarrow {}^4T_{1g}(G)$	—	—	—	—
		538	$^6A_{1g} \rightarrow {}^4T_{2g}(G)$				
		491	$^6A_{1g} \rightarrow {}^4E_g(D)$				

regions for all the complexes could be attributed to the M−O and M−N, respectively.

3.2. Electronic spectra and magnetic moments

The reflectance spectrum of Ti(III) complex shows a broad band in the range 489–532 nm due to $^2T_{2g} \rightarrow {}^2E_g$, transition, in an octahedral symmetry around the Ti(III) ion [34]. The magnetic moment of Ti(III) complex is found to be 1.87 B.M. corresponding to one unpaired electron in an octahedral environment. The reflectance spectrum of Cr(III) complex shows three bands at 580 nm, 411 nm and 262 nm due to $^4A_{2g}(F) \rightarrow {}^4T_{2g}(F)$, $^4A_{2g}(F) \rightarrow {}^4T_{1g}(F)$, and $^4A_{2g}(F) \rightarrow {}^4T_{2g}(P)$, transitions, respectively, suggesting an octahedral environment around the chromium ion. The magnetic moment value 3.97 B.M. is found within the acceptable range for the octahedral geometry.

The ligand field parameters: Dq Racah interelectronic repulsion parameter (B^1), nephelauxetic ratio (β), and % covalency of the metal ligand bond, have been calculated by known relations [35]:

$$E[^4A_{2g}(F) \rightarrow {}^4T_{2g}(F) = 10\,Dq$$

$$15\,B^1 = \nu_3 + \nu_2 - 3\nu_3$$

$$\beta = \frac{B \text{ in the complex}}{B \text{ in free ion}} = \frac{B^1}{B}$$

$$\% \text{ covalency} = (1 - \beta) \times 100.$$

The calculated values of crystal field parameters Dq (1,724 cm^1), B (709 cm^1), β (0.77 cm^{-1}) are also in good agreement with those reported for octahedral Cr(III) complexes (Table 3) [35]. The ν_2/ν_1 ratio is found to be 1.44 which is very close to the value of 1.42 obtained for most of the octahedral complexes. Electronic spectrum of Fe(III) complex shows three d-d bands at 833 nm, 528 nm, and 491 nm, which are assigned to $^6A_{1g} \rightarrow {}^4T_{1g}(G)$, $^6A_{1g} \rightarrow {}^4T_{2g}(G)$, and $^6A_{1g} \rightarrow {}^4E_g(D)$ transitions, respectively, in octahedral geometry. The observed magnetic moment of 5.91 B.M. for Fe(III) complex is in the range expected for high spin octahedral system [36]. The Th(IV) and WO_2(VI) complexes did not show any d-d transitions and are found to be diamagnetic as expected for their electronic configurations and likely to be an octahedral geometry. The electronic spectrum of UO_2(VI) complex shows band at 492 nm due to the ligand to metal charge transfer transition. The UO_2(VI) complex is found to be diamagnetic with coordination number six around the central metal ion.

3.3. SEM

The morphology and particle size of the Schiff base and its Ti(III), Cr(III), Fe(III), Th(III), and UO_2(VI) complexes were characterized by scanning electron microscope (Figures 5(a)–5(e)) and revealed a presence of well-defined crystal structure free from any shadow of metal ion on their external surface. Ti(III) and Fe(III) complexes have stack of globule droplet-like structures while Cr(III), Fe(III), Th(III), and UO_2(VI) complexes have platelet-like structures. The smaller average crystalline size found from XRD also shows that the particles are nanocrystalline phase.

3.4. Powder XRD

The XRD spectrum of H_2L ligand (Figure 6) exhibits sharp peaks indicating the crystalline nature of the ligand. The 2θ

Table 4: Indexed X-ray diffraction data of H_2L ligand.

Peak no.	d (obs.)	d (cal.)	Int. wt.	2θ (obs.)	2θ (cal.)	SinSqTheta*E4 (obs.)	SinSqTheta*E4 (cal.)	h	k	l
1	6.8993	6.9016	1.0	12.82	12.82	124.6	124.6	0	1	0
2	6.0413	6.0335	1.0	14.65	14.67	162.6	163.0	1	1	0
3	4.8151	4.7321	1.0	18.41	18.74	255.9	264.9	0	0	1
4	4.2996	4.2487	1.0	20.64	20.89	320.9	328.7	0	1	1
5	3.9955	3.9845	1.0	22.23	22.29	371.6	373.7	3	1	0
6	3.8048	3.7712	1.0	23.36	23.57	409.8	417.2	4	1	0
7	3.2781	3.2762	1.0	27.18	27.20	552.1	552.8	1	2	0
8	2.8056	2.7930	1.0	31.87	32.02	753.8	760.6	3	2	1
9	2.6953	2.7177	1.0	33.21	32.93	816.7	803.3	6	0	0
10	2.5558	2.5634	1.0	35.08	34.97	908.2	902.9	5	1	1
11	2.2939	2.2941	1.0	39.24	39.24	1127.5	1127.3	6	1	1
12	2.1621	2.1621	1.0	41.74	41.74	1269.1	1269.1	1	3	1
13	2.1162	2.1171	1.0	42.69	42.67	1324.8	1323.7	7	0	1
14	1.9636	1.9644	1.0	46.19	46.17	1538.7	1537.5	1	3	1
15	1.3267	1.3261	1.0	70.98	71.02	3370.5	3373.9	7	0	3

Unit cell data and crystal lattice parameters

$a = 10.3769$ Å $b = 16.9788$ Å	$V = 1175.69$ Å^3
$c = 6.7953$ Å	Crystal system: triclinic
$\alpha = 92.225°$ D	Nature: crystalline
$\beta = 99.964°$ $\gamma = 93.369°$	Particle size = 32.07 nm

values and the indexed X-ray diffraction data corresponding to the prominent peaks have been listed in Table 4. The unit cell data and crystal lattice parameters for the ligand (H_2L) are found to be $a = 10.3769$ Å, $b = 16.9788$ Å, $c = 6.7953$ Å, $\alpha = 92.225°$, $\beta = 99.964°$, $\gamma = 93.369°$, $V = 1175.69$ Å^3 therefore the system is triclinic. X-ray powder pattern of UO_2(VI) complex has been recorded as a representative case and the data are presented in Figure 7. X-ray crystal system has been worked out by trial and error method for finding the best fit between observed and calculated values and the data are given in Table 5. The unit cell parameters values obtained for [UO_2(L)(CH_3OH)] complex are system = triclinic $a = 11.0807$ Å, $b = 13.2768$ Å, $c = 10.6823$ Å, $\alpha = 113.506°$, $\beta = 104.982°$, $\gamma = 91.105°$, $V = 1,377.79$ Å^3. The average crystallite size of the UO_2(VI) complex was calculated from Scherer's formula [37,38,39]. Using the full width at half maximum intensity of the pattern, the average size of the crystal is found to be 44 nm, indicating that the complex is in nanocrystalline phase.

3.5. Thermal analysis

Thermal analyses of ligand and its metal complexes were carried out in the temperature range 40–750 °C in air atmosphere with a heating rate of 10 °C min^{-1} to examine their thermal stability and to investigate the percentage mass loss of compounds. Thermograms are shown in Figure 8 and data is compiled in Table 6. The ligand decomposes in one step with continuous weight loss on increasing temperature with almost no residue at the end. The WO_2(VI), Th(IV), and UO_2(VI) complexes decomposed in two steps whereas Ti(III), Cr(III), and Fe(III) complexes decomposed in three steps. The elimination of coordinated water/methanol molecules takes place in first step in the temperature range 90–194 °C. The slight depression near temperature range 190–218 °C in Ti(II), Cr(III) and Fe(III) complexes after dehydration is due to the loss of coordinated chlorine molecule. After the loss of coordinated water/chloride ion, all the complexes show rapid degradation up to 750 °C. This may be due to the decomposition of organic part of the complex, indicated by the rapid fall in the percentage mass loss. A horizontal plateau on the TG curves for all the complexes indicates the decomposition of the complete organic part of the complexes in the last stage leaving residues as metallic oxide at the higher temperature range. From the TGA results, it is confirmed that the thermal stability of the complexes is higher than its free ligand and the complex is found to have formation of a five-membered chelate ring which may be attributed to the fact that the M−N and M−O bonds are highly polarized [40].

For the thermal degradation data of the complexes, various kinetic and thermodynamic parameters such as activation energy (E_a), frequency factor (Z), entropy (S), enthalpy of activation (ΔH), and Gibbs free energy (ΔG) were evaluated by employing the most popular Coats-Redfern relation [41] and values are given in Table 7. The parameters ΔH, ΔS, and ΔG were calculated by using

Table 5: Indexed X-ray diffraction data of $[UO_2(L^1)(CH_3OH)]$ complex.

Peak no.	d (obs.)	d (cal.)	Int. wt.	2θ (obs.)	2θ (cal.)	SinSqTheta*E4 (obs.)	SinSqTheta*E4 (cal.)	h	k	l
1	12.1158	12.0528	1.0	7.29	7.33	40.4	40.8	0	1	0
2	9.6357	9.5928	1.0	9.17	9.21	63.9	64.5	0	1	1
3	8.5809	8.5685	1.0	10.30	10.31	80.6	80.8	1	1	0
4	6.1245	6.1358	1.0	14.45	14.42	158.2	157.6	1	1	1
5	5.2883	5.3004	1.0	16.75	16.71	212.1	211.2	2	0	0
6	4.8177	4.8367	1.0	18.40	18.33	255.6	253.6	1	0	2
7	3.8064	3.8075	1.0	23.35	23.34	409.5	409.3	2	2	1
8	3.6836	3.6776	1.0	24.14	24.18	437.3	438.7	3	0	1
9	3.3249	3.3230	1.0	26.79	26.81	536.7	537.3	3	0	2
10	3.0223	3.0199	1.0	29.53	29.55	649.5	650.5	2	2	1
11	2.9274	2.9264	1.0	30.51	30.52	692.3	692.8	1	3	1
12	2.5693	2.5680	1.0	34.89	34.91	898.7	899.7	1	5	2
13	2.4018	2.4014	1.0	37.41	37.42	1028.5	1028.8	3	2	4
14	2.2365	2.2357	1.0	40.29	40.31	1186.1	1187.0	4	1	1
15	2.1416	2.1413	1.0	42.16	42.17	1293.6	1293.9	4	1	2
16	2.1007	2.1003	1.0	43.02	43.03	1344.4	1344.9	4	4	2
17	1.9481	1.9470	1.0	46.58	46.61	1563.3	1565.0	3	5	3
18	1.9091	1.9080	1.0	47.59	47.62	1627.8	1629.7	3	4	1
19	1.8889	1.8872	1.0	48.13	48.18	1662.8	1665.8	3	6	2
20	1.8202	1.8202	1.0	50.07	50.07	1790.7	1790.8	5	4	3

Unit cell data and crystal lattice parameters

$a = 11.0800$ Å $b = 13.2700$ Å	$V = 1377.79$ Å^3
$c = 10.6800$ Å	Crystal system: triclinic
$\alpha = 113.500°$ D	Nature: crystalline
$\beta = 104.980°$ $\gamma = 91.105°$	Particle size = 44 nm

the relations $\Delta H = E_a - RT$, $\Delta S = [\ln(Ah/kT) - 1]$, and $\Delta G = \Delta H - T\Delta S$, where k is Boltzmann's constant and h is plank's constant [42,43,44,45]. The reactions are classified on the basis whether they give off heat as exothermic ($\Delta H < 0$) for absorb heat as endothermic ($\Delta H > 0$). Further, the reactions are classified as exergonic ($\Delta G < 0$) where the free energy of the system decreases and endergonic ($\Delta G > 0$) where free energy of the system increases during the course of reaction. The higher value of activation energy of complexes indicates their thermal stability. The results revealed that the activation energy decreases with the increasing radius of metal cation. ΔG is positive for the reaction for which ΔH is positive and ΔS is negative. The reaction for which ΔG is positive and ΔS is negative reflects high thermal stability and unfavorable or nonspontaneous decomposition of the compounds. The estimated thermodynamic activation parameters are indicative of an endothermic process related to an irreversible thermal decomposition, suggesting a better molecular orientation in the activated state. The observed negative values of entropy for the decomposition reaction indicate a more ordered structure for the compound, and the decomposition reactions are slower than normal and also non-spontaneous in nature [46]. The correlations coefficients obtained for the thermal decompositions are lying in the range of 0.915 to 0.998, showing good fit with linear function.

3.6. Solid-state conductivity

The electrical conductivity (σ) of ligand and its complexes was measured as a function of temperature (T) in the temperature range 313–373 K in their compressed pellet form (3 ton cm^{-2}). The values of electrical conductivities (σ) and activation energy (E_a) are listed in Table 1. The electrical conductivity (σ) varies exponentially with the absolute temperature according to the Arrhenius relation $\sigma = \sigma^\circ \exp(-E_a/KT)$, where σ° is constant, E_a is the activation energy of electrical conduction, T is the absolute temperature, and K is the Boltzman constant. A linear dependence of $\log\sigma = f(10^3/T)$, as evident from Arrhenius plot of electrical conductivity (Figure 9), indicates the semiconducting behavior of these compounds [47]. The electrical conductivity value at room temperature lies in the range 7.32×10^{-12} to $7.34 \times 10^{-10}\ \Omega^{-1}\,\text{cm}^{-1}$ and activation energy 0.856–0.440 eV respectively. The observed low value of electrical conductivity of compounds may be attributed to low molecular weight due to which the extent of conjugation becomes low or undesirable morphology due to pressing of the sample into hard brittle pellet form.

Table 6: Thermogravimetric data of metal complexes.

Compound	Temp. range (°C)	% Mass loss		Assignment
		Found	Calcd.	
$[Ti(L)(Cl)(H_2O)_2]$	92–194	9.50	9.54	Loss of 2 moles of coordinated water molecules
	194–218	9.38	9.41	Loss of 1 coordinated chloride ion
	218–750			Delegation
$[Cr(L)(Cl)(H_2O)_2]$	92–194	9.50	9.54	Loss of 2 moles of coordinated water molecules
	194–218	9.38	9.41	Loss of 1 coordinated chloride ion
	218–750			Delegation
$[Fe(L)(Cl)(H_2O)_2]$	90–190	9.20	9.44	Loss of 2 moles of coordinated water molecules
	190–205	9.40	9.31	Loss of 1 coordinated chloride ion
	205–750			Delegation
$[WO_2(L)(H_2O)]$	90–182	3.2	3.6	Loss of 1 mole of coordinated water molecule
	182–650			Delegation
$[Th(L)(NO_3)_2(H_2O)]$	92–194	9.50	9.54	Loss of 1 moles of coordinated water molecules
	194–218	9.38	9.41	Loss of 2 coordinated nitrate ions
	218–750			Delegation
$[UO_2(L)(CH_3OH)]$	105–190	5.8	5.76	Loss of 1 mole of coordinated methanol molecule
	190–680			Delegation

Table 7: Thermal decomposition data of ligand and its complexes.

Compound	Activation energy "E_a" (kJmol^{-1})	Frequency factor "Z" (sec^{-1})	Entropy change "ΔS" (Jmol^{-1}K^{-1})	Enthalpy change "ΔH" (Jmole^{-1})	Free energy change "ΔG" (kJmol^{-1})	Correlation coefficient "r"
H_2L	9.55	9.15×10^4	-270.40	4.6×10^4	165.84	0.914
$[Ti(L)(Cl)(H_2O)_2]$	17.75	2.83×10^2	-242.56	5.8×10^4	172.09	0.998
$[Cr(L)(Cl)(H_2O)_2]$	18.78	2.26×10^3	-263.64	8.3×10^4	185.67	0.919
$[Fe(L)(Cl)(H_2O)_2]$	19.84	3.59×10^2	-248.11	4.2×10^5	207.87	0.987
$[WO_2(L)(H_2O)]$	13.19	1.15×10^2	-241.93	9.2×10^4	207.46	0.968
$[Th(L)(NO_3)_2(H_2O)]$	12.93	7.98×10^3	-253.90	1.3×10^4	188.88	0.978
$[UO_2(L)(CH_3OH)]$	15.21	2.77×10^2	-241.95	6.4×10^5	157.85	0.963

Table 8: Antimicrobial activity of the H_2L ligand and its metal complexes.

Compound	Minimum inhibitory concentration (μg mL^{-1})								
	E. coli (MTCC 443)	*P. aeruginosa* (MTCC 424)	*S. aureus* (MTCC 96)	*B. subtilis* (MTCC 8979)	*E. faecalis* (MTCC 439)	*S. pyogenes* (MTCC 442)	*C. albican* (MTCC 227)	*A. niger* (MTCC 282)	*A. clavatus* (MTCC 1323)
H_2L	12	12	13	11	12	08	11	10	10
$[Ti(L)(Cl)(H_2O)_2]$	15	16	15	19	17	18	12	12	13
$[Cr(L)(Cl)(H_2O)_2]$	15	13	15	18	18	16	15	14	14
$[Fe(L)(Cl)(H_2O)_2]$	15	14	15	18	18	18	12	14	13
$[WO_2(L)(H_2O)]$	14	14	13	16	17	16	13	14	12
$[Th(L)(NO_3)_2(H_2O)]$	15	14	15	17	16	17	12	12	13
$[UO_2(L)(CH_3OH)]$	15	13	14	16	15	16	12	13	15
Ciprofloxacin*	23	25	23	22	20	22	—	—	—
Clotrimazole*	—	—	—	—	—	—	22	22	21

*Standard drug.

3.7. Antimicrobial activity

All the newly synthesized compounds were screened in vitro for their antibacterial and antifungal activities against bacterial strains *S. aureus* MTCC 96, *S. pyogenes* MTCC 442, *B. subtilis* MTCC 8979, *E. coli* MTCC 443, *P. aeruginosa* MTCC 424, and *E. faecalis* MTCC 439 and fungal stains *A. niger* MTCC 282, *A. clavatus* MTCC 1323, and *C. albicans* MTCC 227. The results were recorded for each tested compound as the average diameter of inhibition zones of bacterial growth surrounding the well in mm. The obtained results are presented in Table 8 and shown in Figure 10. It is clear that all of the metal complexes are more potent bactericides and fungicides compared to the free ligand (H_2L). It is also observed from the data that the complexes are slightly more effective towards Gram-positive strains as compared to the Gram-negative

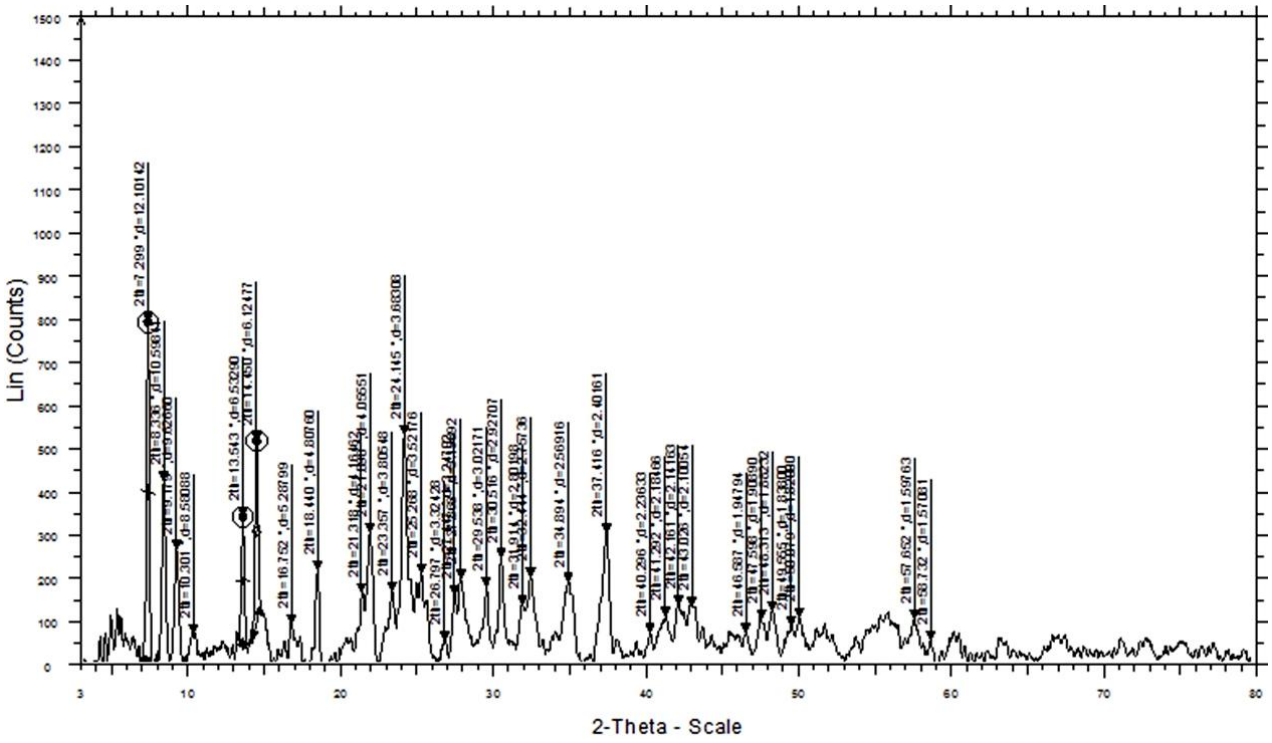

Figure 7: XRD diffractogram of $[UO_2(L)(CH_3OH)]$ complex.

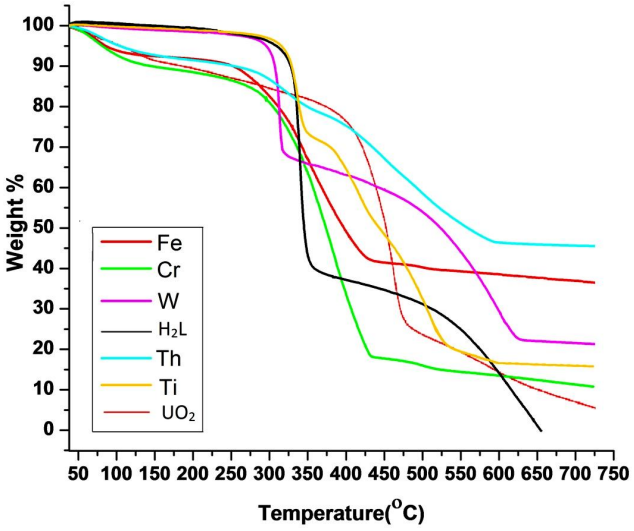

Figure 8: TG curve of ligand and its metal complexes.

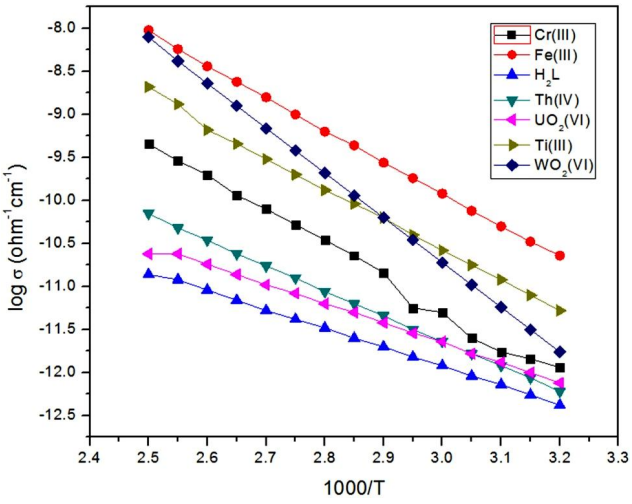

Figure 9: Temperature dependence of $\log\sigma$.

ones, though the level of action of a particular compound within the same type of bacteria is varying. This difference in the activity probably may be attributed to the fact that the cell wall of Gram-positive bacteria have more antigenic properties as the outer lipid membrane is of polysaccharides. Although the complexes showed promising activities against the bacterial strains, however, their activities were found to be less than the standard ciprofloxacin (antibacterial drug) and clotrimazole (antifungal drug). This enhancement in the activity was suggested to be possibly due to an efficient diffusion of the metal complexes into the bacterial cells or interaction with the bacterial cell walls. The results reflect that Ti(III), Cr(III), and Fe(III) complexes exhibited higher activity, while Th(IV), WO_2(VI) and UO_2(VI) complexes showed moderate activity against all bacterial and fungal stains. This growing in the activity could be explained

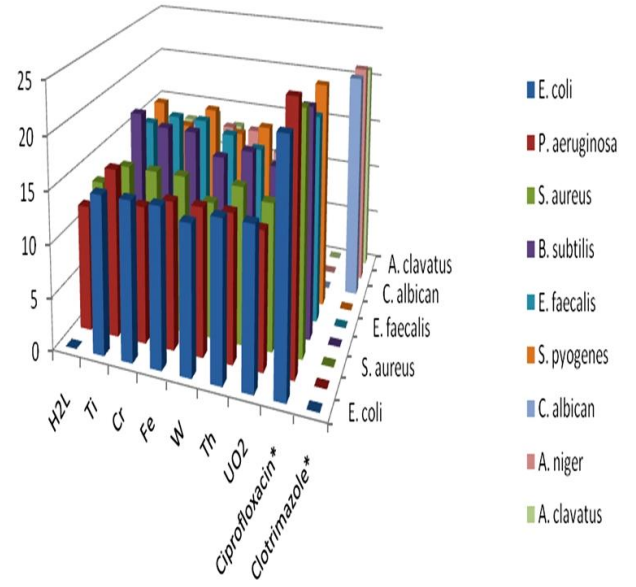

Figure 10: Antimicrobial activity of the H_2L ligand and its metal complexes.

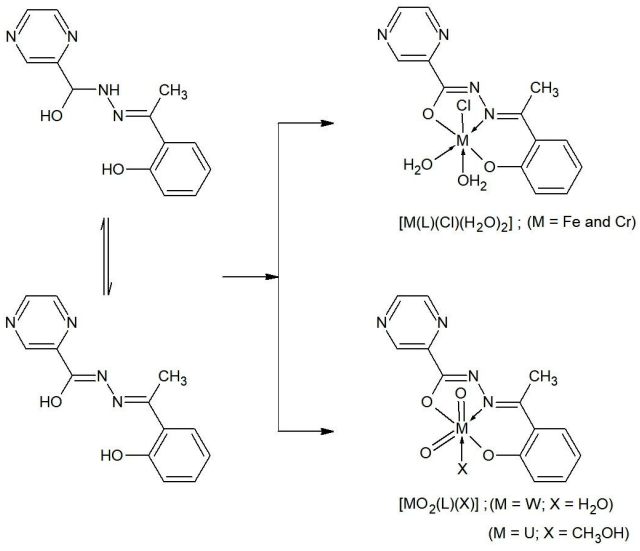

Figure 11: Schematic diagram for complexation processes.

based on the chelation theory [48]. The chelation decreases the polarity of the metal extremely and fundamentally due to the partial involvement of its positive charge with donor groups and possible π-electron delocalization overall chelate rings. The lipid and polysaccharides are some important constituents of cell wall and membranes, which are favorable for metal ion interaction [49,50,51]. Chelation not only can diminish the polarity of the metal ion, but also can raise the lipophilic property of the chelate and the interaction between metal ions and the lipid is preferable. This could lead to the slump of the permeability barrier of the cell resulting in interference with normal cell processes. If the geometry and charge distribution around the molecule are incompatible with geometry and charge distribution around the pores of the bacterial cell wall, then penetration through the wall by the toxic agent cannot take place and this will prevent the toxic reaction within pores. Chelation is not the only criterion for the antimicrobial activity. Some important factors such as the nature of the metal ion, nature of the ligand, coordinating sites, geometry of complex, concentration, hydrophobicity, lipophilicity, and presence of co-ligands have considerable influence on antimicrobial activity. The higher activity of Ti(III), Cr(III), and Fe(III) complexes due to the presence of chlorine group in the structure of complex may be playing an important role towards activity. From the antimicrobial study, it is found that tested compounds possess better antimicrobial activities and also comparable to standards used.

4. Conclusions

In this study, N'-(1-(2-hydroxyphenyl)ethylidene)pyrazine-2-carbohydrazide (H_2L) ligand and its complexes were synthesized and characterized. An octahedral geometry has been inferred for Ti(III), Cr(III), Fe(III), WO_2(VI), Th(IV), and UO_2(VI) complexes where ligand behaves as dibasic tridentate coordinating through phenolate oxygen, azomethine nitrogen, and enolate oxygen atoms to metal ions (Figure 1). The TG analysis indicated that the complexes decompose in two or three overlapping steps where organic parts of the complexes pass though one or two intermediates; finally they converted into the corresponding metal oxide. The solid-state electrical conductivity measurements suggest their semiconducting nature. In vitro biological activity of all newly synthesized compounds exhibited good results with an enhancement of activity on complexation with metal ions. This enhancement in the activity may be attributed to increased lipophilicity of the complexes.

Acknowledgments The authors are thankful to Sophisticated Test & Instrumentation Centre, Cochin, Kerala for providing Powder XRD, TG-DTA, and SEM. Authors are also thankful to Sophisticated Analytical Instrument facility, Punjab University, Chandigarh for providing elemental analysis and IR, ^{1}H NMR, and ^{13}C NMR spectra facility. Sant Gadge Baba Amravati University, Amravati (Maharashtra) for providing laboratory facilities is also gratefully acknowledged.

Conflict of interest The authors declare that they have no conflict of interest.

References

[1] N. Ribeiro, A. M. Galvão, C. S. B. Gomes, H. Ramos, R. Pinheiro, L. Saraiva, et al., *Naphthoylhydrazones: coordination to metal ions and biological screening*, New J Chem, 43 (2019), 17801–17818.

[2] C. J. Dhanaraj, J. Johnson, J. Joseph, and R. S. Joseyphus, *Quinoxaline-based Schiff base transition metal complexes: review*, J Coord Chem, 66 (2013), 1416–1450.

[3] C. W. Dikio, I. P. Ejidike, F. M. Mtunzi, M. J. Klink, and E. D. Dikio, *Hydrazide Schiff bases of acetylacetonate metal complexes: synthesis, spectroscopic and biological studies*, Int J Pharm Pharm Sci, 9 (2017), 257–267.

[4] B. Kirthan, M. Prabhakara, H. Bhojya naik, R. Viswanath, and P. Amith Nayak, *Optoelectronic, photocatalytic and biological studies of mixed ligand Cd(II) complex and its fabricated CdO nanoparticles*, J Mol Struct, 1244 (2021), 130917.

[5] A. D. M. Mohamad, M. J. A. Abualreish, and A. M. Abu-Dief, *Antimicrobial and anticancer activities of cobalt (III)-hydrazone complexes: Solubilities and chemical potentials of transfer in different organic co-solvent-water mixtures*, J Mol Liq, 290 (2019), 111162.

[6] M. D. Altintop, A. Özdemir, G. Turan-Zitouni, S. Ilgin, O. Atli, G. Iscan, et al., *Synthesis and biological evaluation of some hydrazone derivatives as new anticandidal and anticancer agents*, Eur J Med Chem, 58 (2012), 299–307.

[7] G. Le Goff and J. Ouazzani, *Natural hydrazine-containing compounds: Biosynthesis, isolation, biological activities and synthesis*, Bioorg Med Chem, 22 (2014), 6529–6544.

[8] A. S. El-Tabl, M. M. Abd-El Wahed, M. A. Wahba, and M. A. Shebl, *Spectroscopic characterization and cytotoxic activity of new metal complexes derived from (1E, N′Z, N′Z)-N′,N′-bis(2-hydroxybenzylidene)-2-(naphthalen-1-yloxy) acetohydrazonohydrazide*, J Adv Chem, 11 (2015), 3888–3918.

[9] O. Sebastian and A. Thapa, *Schiff base metal complexes of Ni, Pd and Cu*, J Chem Pharm Res, 7 (2015), 953–963.

[10] H. F. Abd El-Halim, G. G. Mohamed, and E. A. M. Khalil, *Synthesis, spectral, thermal and biological studies of mixed ligand complexes with newly prepared Schiff base and 1,10-phenanthroline ligands*, J Mol Struct, 1146 (2017), 153–163.

[11] M. S. Hossain, P. K. Roy, C. M. Zakaria, and M. Kudrat-E-Zahan, *Selected Schiff base coordination complexes and their microbial application: A review*, Int J Chem Stud, 6 (2018), 19–31.

[12] V. R. Avupati, R. P. Yejella, V. R. Parala, K. N. Killari, V. M. Papasani, P. Cheepurupalli, et al., *Synthesis, characterization and in vitro biological evaluation of some novel 1,3,5-triazine-Schiff base conjugates as potential antimycobacterial agents*, Bioorg Med Chem Lett, 23 (2013), 5968–5970.

[13] G. Brađan, B. Čobeljić, A. Pevec, I. Turel, M. Milenković, D. Radanović, et al., *Synthesis, characterization and antimicrobial activity of pentagonal-bipyramidal isothiocyanato Co(II) and Ni(II) complexes with 2,6-diacetylpyridine bis(trimethylammoniumacetohydrazone)*, J Coord Chem, 69 (2016), 801–811.

[14] R. S. Bhaskar, C. A. Ladole, N. G. Salunkhe, and A. S. Aswar, *Synthesis, characterization and biological studies of some transition metal complexes with pyrazine Schiff base hydrazone ligand*, Jordan J Chem, 15 (2020), 61–72.

[15] R. S. Bhaskar, C. A. Ladole, N. G. Salunkhe, J. M. Barabde, and A. S. Aswar, *Synthesis, characterization and antimicrobial studies of novel ONO donor hydrazone Schiff base complexes with some divalent metal (II) ions*, Arab J Chem, 13 (2020), 6559–6567.

[16] B. S. Furniss, A. J. Hannaford, P. W. G. Smith, and A. R. Tatchell, *Vogel's Textbook of Practical Organic Chemistry*, Longman Group, London, 5th ed., 1989.

[17] G. H. Jeffery, J. Bassett, J. Mendham, and R. C. Denney, *Vogel's Quantative Chemical Analysis*, John Wiley & Sons, New York, 5th ed., 1989.

[18] S. B. Yu and R. H. Holm, *Aspects of the oxygen atom transfer chemistry of tungsten*, Inorg Chem, 28 (1989), 4385–4391.

[19] R. S. Bhaskar, N. G. Salunkhe, A. R. Yaul, and A. S. Aswar, *Bivalent transition metal complexes of ONO donor hydrazone ligand: Synthesis, structural characterization and antimicrobial activity*, Spectrochim Acta A Mol Biomol Spectrosc, 151 (2015), 621–627.

[20] D. C. Gross and J. E. DeVay, *Production and purification of syringomycin, a phytotoxin produced by Pseudomonas syringae*, Physiol Plant Pathol, 11 (1977), 13–28.

[21] A. M. Abu-Dief, N. M. El-Metwaly, S. O. Alzahrani, F. Alkhatib, M. M. Abualnaja, T. El-Dabea, et al., *Synthesis and characterization of Fe(III), Pd(II) and Cu(II)-thiazole complexes; DFT, pharmacophore modeling, in-vitro assay and DNA binding studies*, J Mol Liq, 326 (2021), 115277.

[22] A. M. Abu-Dief, L. H. Abdel-Rahman, A. A. Abdelhamid, A. A. Marzouk, M. R. Shehata, M. A. Bakheet, et al., *Synthesis and characterization of new Cr(III), Fe(III) and Cu(II) complexes incorporating multi-substituted aryl imidazole ligand: Structural, DFT, DNA binding, and biological implications*, Spectrochim Acta A Mol Biomol Spectrosc, 228 (2020), 117700.

[23] A. M. Abu-Dief, H. M. El-Sagher, and M. R. Shehata, *Fabrication, spectroscopic characterization, calf thymus DNA binding investigation, antioxidant and anticancer activities of some antibiotic azomethine Cu(II), Pd(II), Zn(II) and Cr(III) complexes*, Appl Organomet Chem, 33 (2019), e4943.

[24] A. M. Abu-Dief, L. H. Abdel-Rahman, M. R. Shehata, and A. A. H. Abdel-Mawgoud, *Novel azomethine Pd (II)- and VO (II)-based metallo-pharmaceuticals as anticancer, antimicrobial, and antioxidant agents: Design, structural inspection, DFT investigation, and DNA interaction*, J Phys Org Chem, 32 (2019), e4009.

[25] P. Jain, D. Kumar, S. Chandra, and N. Misra, *Experimental and theoretical studies of Mn(II) and Co(II) metal complexes of a tridentate Schiff's base ligand and their biological activities*, Appl Organometal Chem, 34 (2020), e5371.

[26] M. R. Maurya, S. Dhaka, and F. Avecilla, *Synthesis, characterization, reactivity and catalytic activity of dioxidomolybdenum(VI) complexes derived from tribasic ONS donor ligands*, Polyhedron, 81 (2014), 154–167.

[27] M. R. Maurya, B. Sarkar, F. Avecilla, S. Tariq, A. Azam, and I. Correia, *Synthesis, characterization, reactivity, catalytic activity, and antiamoebic activity of vanadium(V) complexes of ICL670 (deferasirox) and a related ligand*, Eur J Inorg Chem, 2016 (2016), 1430–1441.

[28] B. Samanta, J. Chakraborty, S. Shit, S. R. Batten, P. Jensen, J. D. Masuda, et al., *Synthesis, characterisation and crystal structures of a few coordination complexes of nickel(II), cobalt(III) and zinc(II) with N′-[(2-pyridyl)methylene]salicyloylhydrazone Schiff base*, Inorganica Chim Acta, 360 (2007), 2471–2484.

[29] N. Biswas, S. Bera, N. Sepay, T. K. Mukhopadhyay, K. Acharya, S. Ghosh, et al., *Synthesis, characterization, and cytotoxic and antimicrobial activities of mixed-ligand hydrazone complexes of variable valence VO^{z+} ($z = 2,3$)*, New J Chem, 43 (2019), 16714–16729.

[30] S. P. McGlynn and J. K. Smith, *The electronic structure, spectra, and magnetic properties of actinyl ions: Part II. Neptunyl, and the ground states of other actinyls*, J Mol Spectrosc, 6 (1961), 188–198.

[31] L. H. Jones, *Determination of U-O bond distance in uranyl complexes from their infrared spectra*, Spectrochim Acta, 15 (1959), 409–411.

[32] M. K. Rahangdale, A. R. Yaul, G. B. Pethe, and A. S. Aswar, *Synthesis, physicochemical and antibacterial studies of transition metal chelates involving tetradentate Schiff base*, J Indian Chem Soc, 91 (2014), 1891–1898.

[33] D. Kumar, A. Syamal, and A. K. Singh, *Synthesis and characterization of manganese(II), cobalt(II), nickel(II), copper(II), zinc(II), cadmium(II), iron(III), zirconium(IV), dioxomolybdenum(VI) and dioxouranium(VI) coordination compounds of polystyrene-supported tridentate dibasic Schiff base derived from semicarbazide and 3-formylsalicylic acid*, Indian J Chem, 42A (2003), 280–286.

[34] R. K. Rastogi, S. Sharma, G. Rastogi, and A. K. Singh, *Synthesis and characterization of Ti (III), V (III), Vo (IV), MoO (V), Fe (II) and Fe (III) complexes of benzil-*2,4*-dinitrophenyl hydrazone p-bromo aniline*, Green Chem Technol Lett, 2 (2016), 177–179.

[35] J. D. Lee, *Concise Inorganic Chemistry*, Chapman and Hall, London, 4th ed., 1991.

[36] V. P. Singh, S. Singh, D. P. Singh, P. Singh, K. Tiwari, M. Mishra, et al., *Synthesis, spectral and single crystal X-ray diffraction studies on Co(II), Ni(II), Cu(II) and Zn(II) complexes with o-amino acetophenone benzoyl hydrazone*, Polyhedron, 56 (2013), 71–81.

[37] L. H. Abdel-Rahman, A. M. Abu-Dief, R. M. El-Khatib, and S. M. Abdel-Fatah, *Some new nano-sized Fe(II), Cd(II) and Zn(II) Schiff base complexes as precursor for metal oxides: Sonochemical synthesis, characterization, DNA interaction, in vitro antimicrobial and anticancer activities*, Bioorg Chem, 69 (2016), 140–152.

[38] W. S. Mohamed and A. M. Abu-Dief, *Synthesis, characterization and photocatalysis enhancement of Eu_2O_3-ZnO mixed oxide nanoparticles*, J Phys Chem Solids, 116 (2018), 375–385.

[39] E. M. M. Ibrahim, A. M. Abu-Dief, A. Elshafaie, and A. M. Ahmed, *Electrical, thermoelectrical and magnetic properties of approximately* 20*-nm Ni-Co-O nanoparticles and investigation of their conduction phenomena*, Mater Chem Phys, 192 (2017), 41–47.

[40] M. L. Dianu, A. Kriza, and A. M. Musuc, *Synthesis, spectral characterization, and thermal behavior of mononuclear Cu(II), Co(II), Ni(II), Mn(II), and Zn(II) complexes with* 5*-bromosalycilaldehyde isonicotinoylhydrazone*, J Therm Anal Calorim, 112 (2013), 585–593.

[41] A. Coats and J. Redfern, *Kinetic parameters from thermogravimetric data*, Nature, 201 (1964), 68–69.

[42] L. H. Abdel-Rahman, M. S. S. Adam, A. M. Abu-Dief, and A. A. H. Abdel-Mawgoud, *Catalytic potential of mononuclear Cr(III)-imine complexes for selective oxidation of benzyl alcohol by aqueous H_2O_2*, J Transit Met Complexes, 2 (2019), art236077.

[43] A. M. Abu-Dief, R. M. El-khatib, F. S. Aljohani, S. O. Alzahrani, A. Mahran, M. E. Khalifa, et al., *Synthesis and intensive characterization for novel Zn(II), Pd(II), Cr(III) and VO(II)-Schiff base complexes; DNA-interaction, DFT, drug-likeness and molecular docking studies*, J Mol Struct, 1242 (2021), 130693.

[44] L. H. Abdel-Rahman, A. M. Abu-Dief, F. M. Atlam, A. A. H. Abdel-Mawgoud, A. A. Alothman, A. M. Alsalme, et al., *Chemical, physical, and biological properties of Pd(II), V(IV)O, and Ag(I) complexes of N_3 tridentate pyridine-based Schiff base ligand*, J Coord Chem, 73 (2020), 3150–3173.

[45] M. A. A. A. El-Remaily, A. M. M. Soliman, M. E. Khalifa, N. M. El-Metwaly, A. Alsoliemy, T. El-Dabea, et al., *Rapidly, highly yielded and green synthesis of dihydrotetrazolo[*1,5*-a]pyrimidine derivatives in aqueous media using recoverable Pd (II) thiazole catalyst accelerated by ultrasonic: Computational studies*, Appl Organomet Chem, 36 (2022), e6320.

[46] R. G. Frost, A. A. und Pearson, *Kinetics and Mechanism*, John Wiley & Sons, New York, 1961.

[47] K. K. Narang, K. B. Singh, and M. K. Singh, *Synthesis, characterization, XRD, magnetic moments, electronic and IR spectra of chromium(III) malondihydrazide azide/sulphate complexes*, Synth React Inorg Met-Org Chem, 23 (1993), 1547–1559.

[48] I. Babahan, S. Emirdag-Öztürk, and E. Poyrazoglu-Çoban, *Spectroscopic and biological studies of new mononuclear metal complexes of a bidentate NN and NO hydrazone-oxime ligand derived from egonol*, Spectrochim Acta A Mol Biomol Spectrosc, 141 (2015), 300–306.

[49] E. T. Aljohani, M. R. Shehata, F. Alkhatib, S. O. Alzahrani, and A. M. Abu-Dief, *Development and structure elucidation of new VO^{2+}, Mn^{2+}, Zn^{2+}, and Pd^{2+} complexes based on azomethine ferrocenyl ligand: DNA interaction, antimicrobial, antioxidant, anticancer activities, and molecular docking*, Appl Organomet Chem, 35 (2021), e6154.

[50] M. Zaib, T. Shahzadi, I. Muzammal, and U. Farooq, *Catharanthus roseus extract mediated synthesis of cobalt nanoparticles: evaluation of antioxidant, antibacterial, hemolytic and catalytic activities*, Inorg Nano-Metal Chem, 50 (2020), 1171–1180.

[51] L. H. Abdel-Rahman, A. M. Abu-Dief, and A. A. H. Abdel-Mawgoud, *Development, structural investigation, DNA binding, antimicrobial screening and anticancer activities of two novel quari-dentate VO(II) and Mn (II) mononuclear complexes*, J King Saud Univ Sci, 31 (2019), 52–60.